Materials Science & Engineering A 854 (2022) 143782

Contents lists available at ScienceDirect

Materials Science & Engineering A

journal homepage: www.elsevier.com/locate/msea

# Microstructure and mechanical properties of dense $Si_3N_4$ ceramics prepared by direct coagulation casting and cold isostatic pressing

Hande Marulcuoglu [a,*], Ferhat Kara [b]

[a] Abdullah Gül University, Faculty of Engineering, Department of Nanotechnology Engineering, 38080, Kayseri, Turkey
[b] Eskisehir Technical University, Faculty of Engineering, Department of Materials Science and Engineering, 26480, Eskisehir, Turkey

ARTICLE INFO

*Keywords:*
$Si_3N_4$
Direct coagulation casting
Mechanical properties
Microstructure
Cold isostatic press

ABSTRACT

Complex shaped dense $Si_3N_4$ ceramics were produced by using direct coagulation casting technique via dispersant reaction method of $Si_3N_4$ suspension, followed by gas pressure sintering. The effects of solid content of the suspension, additional cold isostatic pressing of the cast parts, and sintering behaviour and on the mechanical reliability of silicon nitride ceramics were investigated. It was observed that all slurries exhibited rheological properties suitable for casting in the range of 44–50 vol.% solid concentrations. Nevertheless, higher solid concentration suspensions resulted in smaller floc size and thus better green microstructures. Parts shaped by direct coagulation casting at all the solid loadings had relatively low strength and reliability after sintering. However, application of additional cold isostatic pressing to the cast parts increased the strength and, particularly, reliability. Dense $Si_3N_4$ ceramics with relative density above 99.5%, average bending strength 760 ± 39 MPa and Weibull module 23.5 had been obtained with 50 vol.% solids content after DCC + CIP process.

## 1. Introduction

Silicon nitride ($Si_3N_4$) ceramics, having numerous advantageous properties such as exceptional mechanical behaviours, wear resistance, good thermal shock and corrosion resistance, are commonly being utilised for various structural applications. These applications include automotive engine parts, ball bearings, ceramic armour, turbine blades, heat exchangers and cutting tools [1–5]. Traditional shaping methods such as slip casting, injection molding, extrusion and dry pressing have been commonly used to produce $Si_3N_4$ ceramics [6,7]. In addition, gelcasting and direct coagulation casting (DCC) have also been developed as alternative shaping methods in recent years, particularly for the complex shaped $Si_3N_4$ ceramics in order to reduce or avoid green and sintered machining costs [6,7].

Gelcasting is a novel colloidal shaping method which is based on the formation of three dimensional network of some organic gel forming additives [8,9]. However, the highly neurotoxic organic systems are often used and the binder removal process takes longer time. This has prevented it to be commonly used in industrial applications [10,11]. On the other hand, DCC relies on the coagulation of a stable colloidal suspension at high solid concentration with the use of a small amount of suitable additives in the suspension which causes its destabilisation [12]. The coagulation process in DCC occurs by either increasing ionic strength which compresses the electrical double layer or shifting the pH towards the isoelectric point (IEP) of the suspensions [13–16]. In both cases, attractive forces between particles in the suspension increase and turn a stable suspension from the liquid condition into a solid particle network [7,12,16].

In order to assess the effectiveness of the gelcasting and DCC on mechanical properties, several studies have been made [15,17–21]. Gan et al. [15] shaped $Si_3N_4$ ceramics by DCC via dispersant reaction, where they used tetramethylammonium hydroxide (TMAH) as a dispersant and glycerol diacetate as a reactant for TMAH, and measured the flexural strength after presssureless sintering and hot pressing. The authors reported that the flexural strength of the DCC $Si_3N_4$ after pressureless sintering to 98.8% relative density was 817 ± 75 MPa, which was comparable to the flexural strength of 911 ± 40 MPa of the hot pressed counterpart. Gan et al. [17] prepared SiC ceramics by DCC via dispersant reaction and obtained flexural strength of 697 ± 30 MPa of dense SiC ceramics. In another study, Wu et al. [18] used spark plasma sintering to sinter DCC shaped $Si_3N_4$ ceramic and obtained fracture toughness and hardness values of 8.5 MPa $m^{1/2}$ and 17.5 ± 1.0 GPa, respectively. In a recent study, Liu et al. [19] produced $Si_3N_4$ ceramics by DCC via increasing ionic strength and reported that the ceramic parts had

* Corresponding author.
*E-mail address:* hande.marulcuoglu@agu.edu.tr (H. Marulcuoglu).

https://doi.org/10.1016/j.msea.2022.143782
Received 29 April 2022; Received in revised form 27 July 2022; Accepted 7 August 2022
Available online 13 August 2022

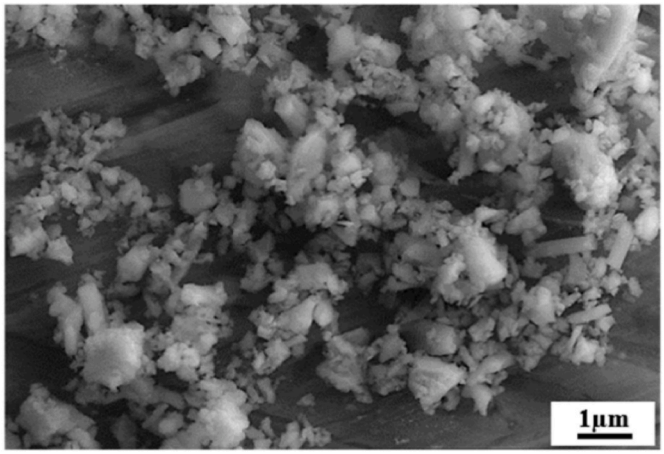


**Fig. 1.** SEM image of the silicon nitride powder [25].

homogeneous microstructure with flexural strength of 758.4 MPa and fracture toughness of 6.3 MPa $m^{1/2}$. Zhang et al. [20] produced SiC ceramics by gelcasting and pressureless sintering. They determined flexural strength and Weibull modulus as 531 ± 38 MPa and 8.11, respectively. In another study, Zhang et al. [21] fabricated the silicon carbide ceramics by gelcasting and pressureless sintering and reported flexural strength as 637 ± 156 MPa. Being a similar technique to DCC, similar strength values were also reported for the $Si_3N_4$ ceramics shaped by the gelcasting method by various authors who also included reliability data in their works [22–24]. Huang et al. [22] reported that surface oxidation of $Si_3N_4$ powder by thermal treatment is needed in order to avoid the reaction between $Si_3N_4$ powder (and free Si powder, if exists in $Si_3N_4$ powder) and water, producing $NH_3$ (g) (and $H_2$ (g) in the case of free Si) which causes the formation of large pores in the green body. In this way, they were able to get dense $Si_3N_4$ ceramics with the flexural strength and Weibull modulus of 785 MPa and 11.8, respectively. Huang et al. [23] prevented the reaction between $Si_3N_4$ and water by coating $Si_3N_4$ powder by $Y_2O_3$ and $Al_2O_3$ sintering additives by precipitating them on the surfaces of $Si_3N_4$ particles from Y and Al containing salts. This approach prevented the formation of large bubbles in the green bodies associated with $NH_3$ (g) evolution during gelcasting and resulted in dense $Si_3N_4$ ceramics with the flexural strength and Weibull modulus of 840 MPa and 15.5, respectively. Zhou et al. [24] also proposed an oxidation treatment of $Si_3N_4$ powder at 600 °C to avoid bubble formation during gel casting and reported 814 MPa flexural strength and 12.4 Weibull modulus and additional cold isotatic pressing of the gelcast green parts further improved the strength to 867 MPa and Weibull modulus to 15.1. The cold isostatic pressing was claimed to remove some larger pores which may remain in the green body during the gelcasting.

With respect to direct coagulation casting, although excellent strength values of DCC cast $Si_3N_4$ were reported by Gan et al. [15] and Liu et al. [19] as mentioned above, there has been no study on the reliability of DCC shaped $Si_3N_4$ ceramics. It also appears from the gel casting studies that large pores due to bubble formation during casting is a concern in colloidal suspension based shaping techniques, particularly for $Si_3N_4$ ceramics [22–24]. Therefore, in this study, an attempt has been made to determine viability of the DCC method to fabricate high strength $Si_3N_4$ ceramics with high reliability. For this, $Si_3N_4$ green parts produced by the DCC method with and without additional cold isostatic pressing (CIP) were sintered by gas pressure sintering and mechanical property comparisons including Weibull modulus ($m$) were made.

## 2. Experimental procedure

### 2.1. Materials

A commercial α-$Si_3N_4$ powder (P95H, VestaSi Europe AB, Sweden) which was produced by direct nitridation of silicon was used in this study in the as-received state with no further treatment. Fig. 1 shows a scanning electron microscopy (SEM) image of the powder. The average particle size ($D_{50}$) of the powder was approximately 0.9 µm and spesific surface area was about 11 $m^2/g$, as quoted by the manufacturer. It contained 0.2% free silicon and 0.5% oxygen. $Al_2O_3$ (99.9%, Alcoa-A16SG, USA) and $Y_2O_3$ (99.99%, REEtec AS, Norway) powders were used as sintering additives. Tetramethylammonium hydroxide (TMAH, 10 wt.% solids content) was used as the dispersant and glycerol diacetate (GDA) (Alfa Aesar, USA) was used as the coagulation agent.

### 2.2. Production of $Si_3N_4$ ceramics

Silicon nitride suspensions at different solid concentrations (44–52 vol.%) were prepared through ball milling of the $Si_3N_4$ powder and sintering additives (2 wt.% $Al_2O_3$ and 5 wt.% $Y_2O_3$) in distilled water in a polyethlene jar for 72 h by using small amount of silicon nitride balls (The mass ratio between grinding medium and $Si_3N_4$ powder was 1:5). TMAH (0.4 wt.% on dry weight basis) was used as deflocculant. This process is not only facilitated intimate mixing of the $Si_3N_4$ powder and additives without substantial grinding due to less ball charge but also hydrolysed all unreacted free silicon which is present in the as-received $Si_3N_4$ powder. It was obderved that extensive bubble formation was observed in the green parts when the milling time was shorther (e.g. 12 h) as a result of the reaction between free Si and water, generating hydrogen gas. The pH value of suspension was about 10.5 after ball milling. The prepared suspensions were degassed under vacuum condition for about 30 min before the coagulation agent (GDA) was added. Then, GDA (2 vol.%) was added into the slurries and mechanically mixed for approx. 3 min for homogenization under room conditions. The suspensions were then poured into a non-porous mould. The mould was closed to prevent water evaporation and put into an oven at 60 °C for 1.5 h for coagulation followed by demoulding. The wet green bodies were dried at 60 °C for 24 h after demoulding. Some of the dried green specimens were subjected to an additional cold isostatic pressing (CIP) for 5 min under 200 MPa. The dried and CIPed samples were debinded in an atmosphere furnace with a heating rate of 3 °C/min to 550 °C with 1 h dwell time at this temperature. The debinded silicon nitride green bodies were then sintered by using gas pressure sintering (GPS) furnace (FCT Anlagenbau GmbH) at 1950 °C for 2 h under 95 bar $N_2$+Ar gas mixture (20% $N_2$). The heating rate was 10 °C/min during sintering.

### 2.3. Characterisation of the materials

The zeta potential of the silicon nitride suspension at a solid loading of 0.05 wt.% with and wihtout TMAH addition was measured using Zetasizer (Malvern Inst.). 1 M HCl and 1 M NaOH were used to adjust the pH value. Rheological behaviours of the silicon nitride slurries were characterised using rheometer (AntonPaar MCR 102) with parallel plate measuring tip (PP25) under ambient conditions. The viscosity measurements were carried out in the range of 0–100 $s^{-1}$ shear rates. The phase composition of both the green and the sintered bodies was determined using X-ray difractometer (XRD, Rigaku Miniflex 600, Cu $K_\alpha$). Density of the green bodies were calculated using the dimensions and weight of rectangular spacimens by a micrometer. Densities of the sintered bodies were measured by the Archimedes method. Bending strength of the sintered specimens prepared by using different solid concentration slurries were determined by using four-point bending test of 3 × 4 × 50 $mm^3$ samples (Instron-M10 25590). Cross-head speed of 0.5 mm/min and a span of 20 mm was used in accordance with ASTM standards (C1161-18). In order to obtain average value, at least 10

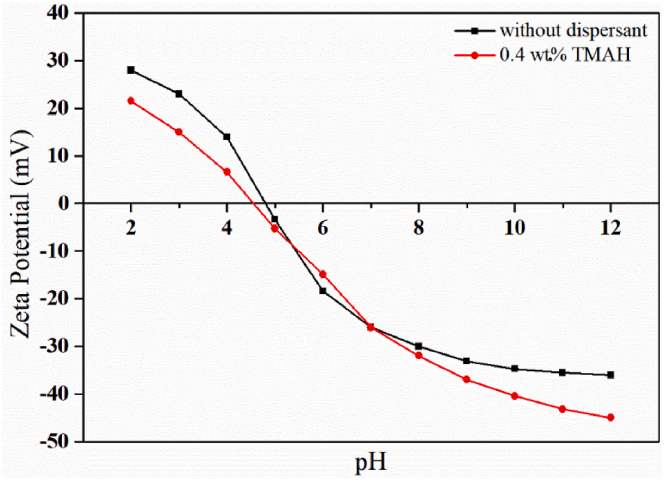


**Fig. 2.** Change in zeta potential of $Si_3N_4$ suspensions with pH.

measurements were taken for each sample group. Before the measurements, the samples were ground and then subjected to heat treatment at 1000 °C for 1 h in static air in an atmospheric furnace in order to heal any surface defects that may be present due to the grinding. Vickers hardness and fracture toughness of the sintered samples were measured by indentation technique (Emco-Test) by using 10 kg load for 10 s. In order to obtain statistical results, at least 5 measurements were made from each sample. Fracture toughness values were calculated by using the Niihara equation [26]. Fracture surfaces of green and sintered bodies were examined by scanning electron microscopy (SEM, Zeiss, SUPRA 50 VP) under secondary electron imaging mode while the polished surfaces of the sintered specimens were examined by using backscattered electron imaging mode.

## 3. Results and discussion

### 3.1. Rheological behaviour of $Si_3N_4$ slurries

The surface charge density is very important in determining the particle distribution and stability in colloidal processes. The zeta potential curves of $Si_3N_4$ suspensions without and with 0.4 wt.% TMAH addition, are shown in Fig. 2. The isoelectric point (IEP) of the $Si_3N_4$ suspension without dispersant addition is at pH 4.8. Above this IEP value, the suspension shows a negative zeta potential that increases with the pH value of the dispersing medium. The highest zeta potential is about −35 mV at a pH range of 10–12. There are two different groups on

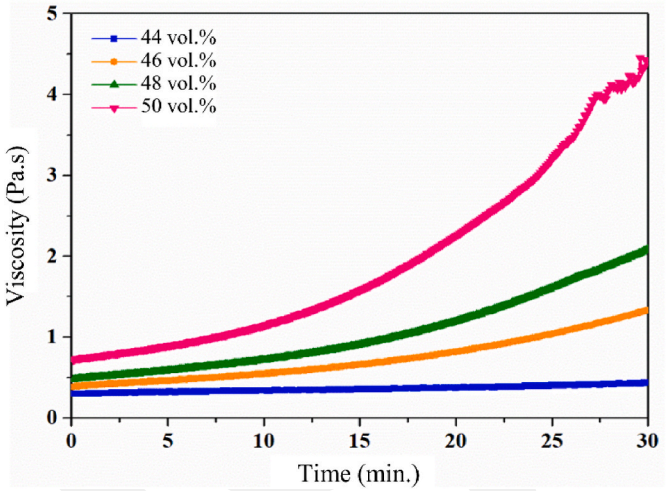


**Fig. 4.** Effect of time on viscosity of different solid loading suspensions containing 2 vol.% GDA at a shear rate of 10 $s^{-1}$.

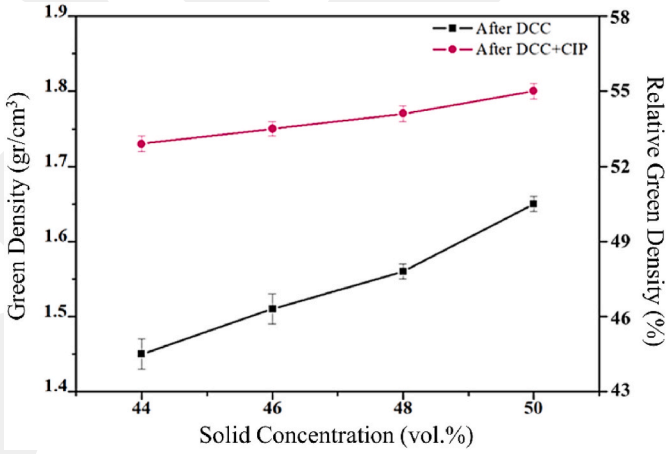


**Fig. 5.** Effect of solid content on the green densities of DDC and DCC + CIP $Si_3N_4$ green bodies. (For interpretation of the references to colour in this figure legend, the reader is referred to the Web version of this article.)

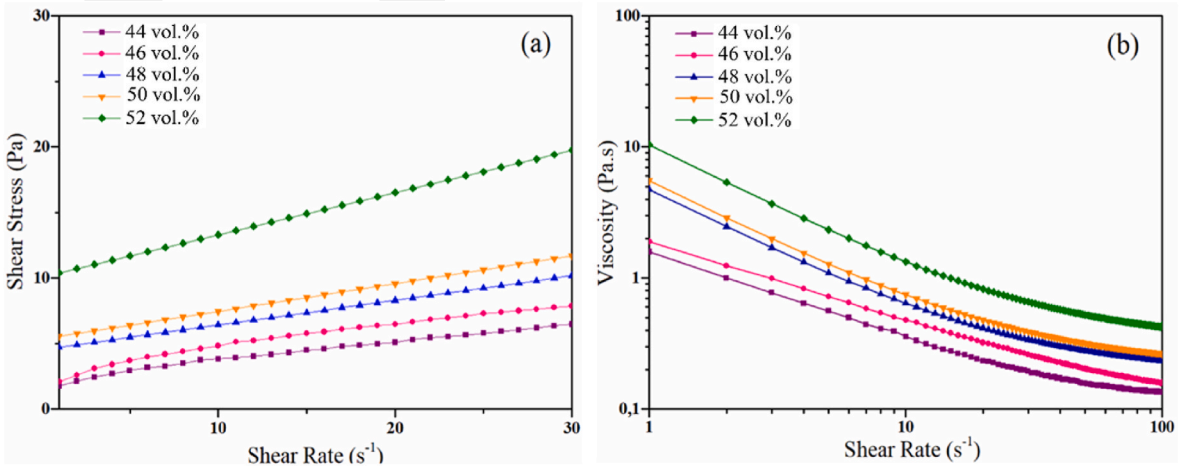


**Fig. 3.** The rheological behaviours of $Si_3N_4$ suspensions depending on solid loadings (a) shear stress-shear rate; (b) viscosity-shear rate.

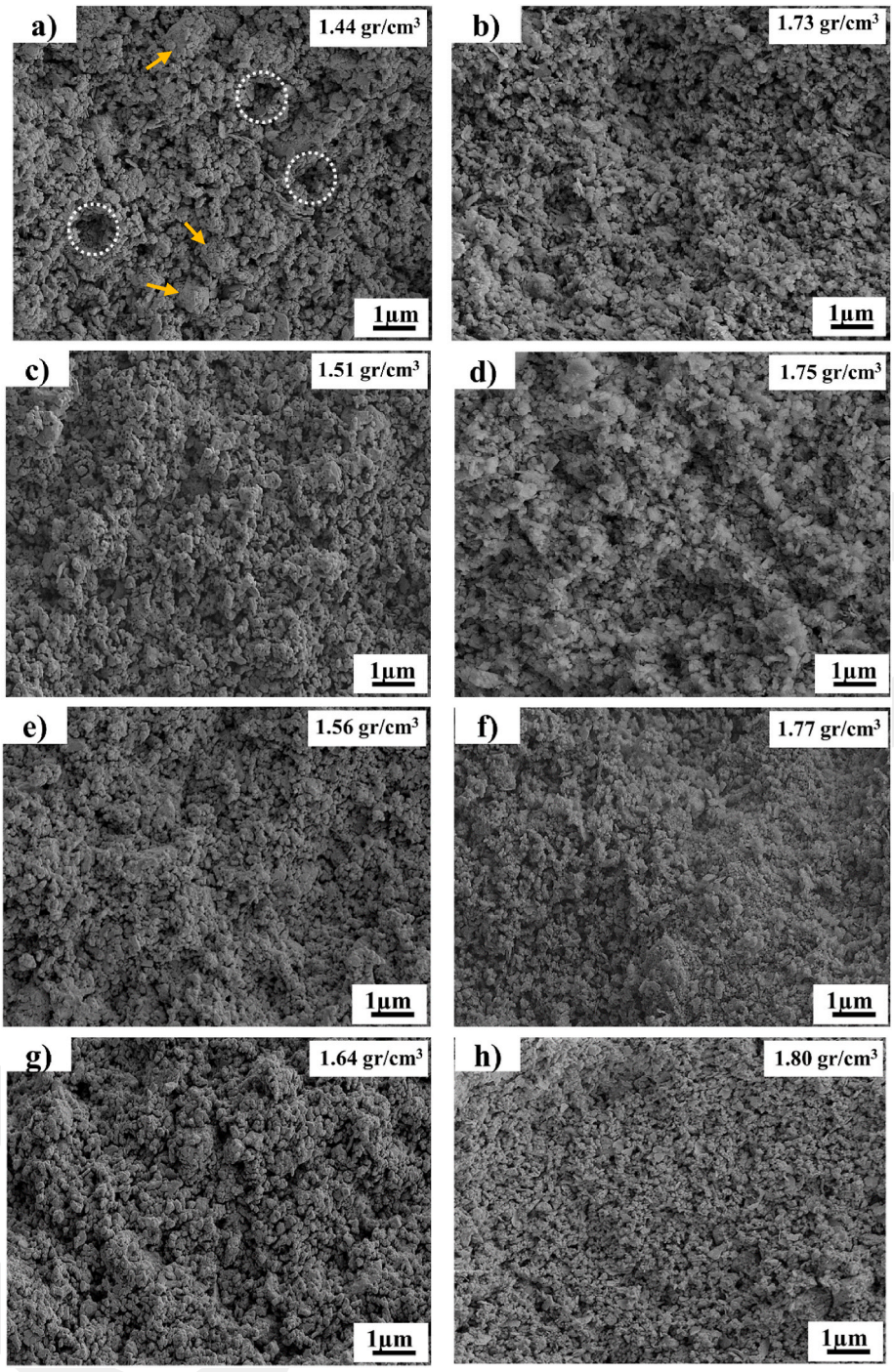


**Fig. 6.** SEM images of $Si_3N_4$ green bodies prepared by DCC method (After DCC; a-c-e-g: 44, 46, 48, 50 vol.%, After DCC + CIP; b-d-f-h: 44, 46, 48, 50 vol.%). Circles in (a) indicate pores and arrows indicate aggregates.

the $Si_3N_4$ particle surface: silanol groups (Si–OH) and silylamine groups (Si–$NH_2$). It is possible for these groups to be ionized in aqueous suspensions. The ionization depends on the pH value of the suspensions. The presence of silanol groups results in a low $pH_{iep}$ and the presence of amine groups results in a high $pH_{iep}$. Depending on the density of the surface groups, the $pH_{iep}$ in the range of 3–9 may observed for silicon nitride [27,28]. Due to the low IEP point, it can be said that silanol groups are dominant on the particle surfaces. With the addition of 0.4 wt.% TMAH, IEP is reduced to pH 4.5 while the highest zeta-potential achieved was −45 mV at a pH range of 10–12. TMAH is a strong base and provides effective electrostatic stabilization of silicon nitride suspensions [29–32] which causes the dissociation of the silanol groups and creates more negative charges on the silicon nitride particle surface [29]. Although the IEP of the $Si_3N_4$ suspension has displaced towards the acidic direction after the dispersant addition, the pH value corresponding to the max. zeta potential is still in a pH range of 10–12. High zeta potential means to high charge density on particle surfaces, and accordingly a good colloidal stabilization occurs due to increased repulsion force between equally charged particles. Therefore, the optimum fluidity of the $Si_3N_4$ suspension is expected to be achieved at a pH range of 10–12.

In shaping by DCC method, rheology of suspensions is an important parameter for obtaining high density ceramics with ideal microstructure and properties [18,33]. Ideally, low viscosity suspensions with as high

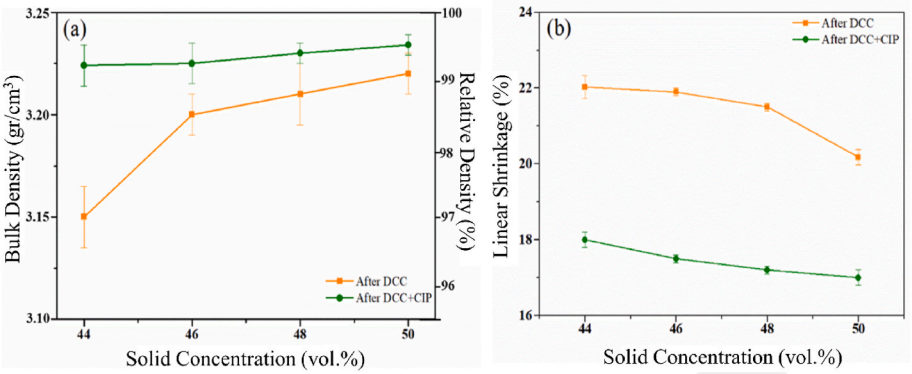


**Fig. 7.** Effect of the suspension solid concentration on (a) sintered bulk density and (b) linear shrinkage of DCC and DCC + CIP bodies.

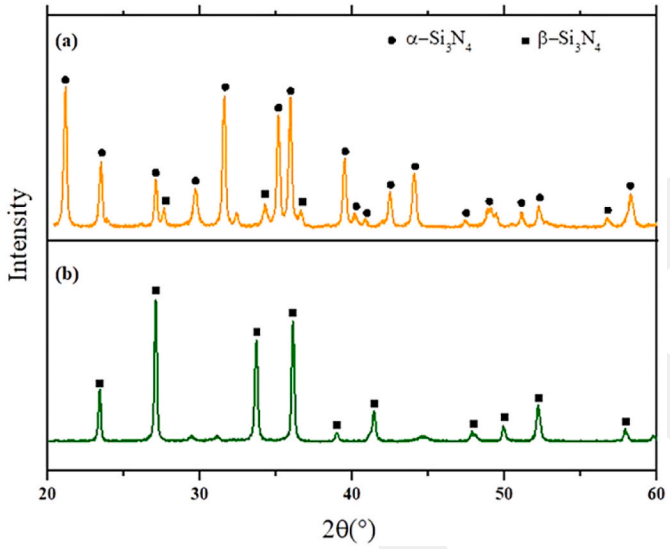


**Fig. 8.** XRD patterns of (a) green and (b) sintered bodies of $Si_3N_4$ prepared with 50 vol.% solid content. (For interpretation of the references to colour in this figure legend, the reader is referred to the Web version of this article.)

solid loading as possible are preferred in casting [15]. The viscosities of $Si_3N_4$ suspensions with different solid concentration in the range of 44–52 vol.% is given in Fig. 3 as a function of shear rate. With the increase in shear rate, the shear stress increased and the viscosity decreased (Fig. 3a and b). All the slurries show shear thining behaviour. Although viscosities of the suspensions are rather high at low shear rates, they are reduced more or less logorithmically with increasing shear rate. Typical shear rates experienced in slow mixing and pouring conditions during suspension preparation are in the range of 10 $s^{-1}$ and the suspension viscosity should be below 1 Pa s at this shear rate for good mould filling during casting. The viscosity of the $Si_3N_4$ suspensions at 10 $s^{-1}$ increased approx. from 0.36 Pa•s to 1.34 Pa•s with increasing solid concentration from 44 to 52 vol.%. Therefore, 50 vol.% solid loading (0.75 Pa•s at 10 $s^{-1}$) is about the limit for good fluidity for casting complex shape process according to Fig. 3.

Fig. 4 shows change in viscosity at a shear rate of 10 $s^{-1}$of suspensions with time at different solid loadings (44–50 vol.%) after adding 2 vol.% GDA at room temperature. For all the solid loadings, the slurry viscosities increase with time and the viscosity increase becomes faster with the increasing suspension solid loading due to the less distance between particles in the suspension. After a certain time, the suspension turn into a rigid green body. The reason behind the increase in viscosity and subsequent formation of a rigid body is as follows: GDA hydrolyzes under alkaline conditions and produces acetatic acid [34]. TMAH, used as the dispesant, is a strong base and the acid-base reaction between acetic acid and TMAH takes place according to the reaction given below [15]:

$$(CH_3)_4NOH + CH_3COOH \rightarrow CH_3COON(CH_3)_4 + H_2O \quad (1)$$

This reaction gradually reduces the amount of the dispersant and hence of the charges on the silicon nitride particles surfaces and as a result coagulation occurs.

### 3.2. *Properties of $Si_3N_4$ green bodies and their sintering behaviour*

The green body properties have significant effect on the final product properties. Fig. 5 shows the effect of the suspension solid content on the green density of the as-cast specimens and after CIP. Green densities of the as-cast samples closely resembled the slurry particle volume loading, being fractionally higher than the slurry particle volume loading, due to a small amount of linear drying shrinkage (measured as 1.2–1.7%). As the solid concentration increased from 44 vol.% to 50 vol.%, the relative green densities increased from approximately 44.4%–50.5% linearly. This indicates that the slip structure kept almost unchanged during coagulation process. Cold isostatic pressing of the DCC green parts increases the green densities further by reducing interparticle spacing and pore size. Relative green density of the samples prepared from 44 vol.% and 50 vol.% suspensions increased from 44.4% to 50.5%–53.3% and 55.5%, respectively.

Fig. 6 shows the secondary electron images of the fractured surfaces of the dried DCC green parts and after CIP. It is noticeable that DCC green parts (Fig. 6a,c,e,g), particularly the one with 44 vol.%, have easily distinguishable aggregates (arrowed in Fig. 6a) and some larger size pores than interparticle porosity (marked with light circles in Fig. 6a) among these aggregates. The aggregates seem to get smaller and are not easily evident as the particle volume loading of the suspension increases. The formation of these aggregates must be due to the floc formation just before solidification of the suspension as the interparticle forces are reduced with the progress of dispersant reaction. The reason why they are particularly evident in the lowest particle volume loading suspension could be the higher degree of freedom of the particles at low volume loadings so that the primary particles can form larger flocs. CIP causes the collapse of the aggregates as can be seen in Fig. 6b,d,f,h and thus increases the green density by further reducing the interparticle spacing and size of the larger pore. Nevertheless, it appears that the aggregates somehow reduce the packing density and homogeneity of the green bodies and they can be the reason behind the lower green densities of the CIPed green parts at lower solid loadings (Fig. 5).

Fig. 7a shows the densification behaviour of the different volume loading suspensions after DCC and after DCC + CIP while Fig. 7b gives corresponding sintering shrinkages. Linear shrinkage values up to 22% of DCC samples could be reduced to less than 18% with further CIP. Only 97% relative bulk density was achieved when 44 vol.% suspension is

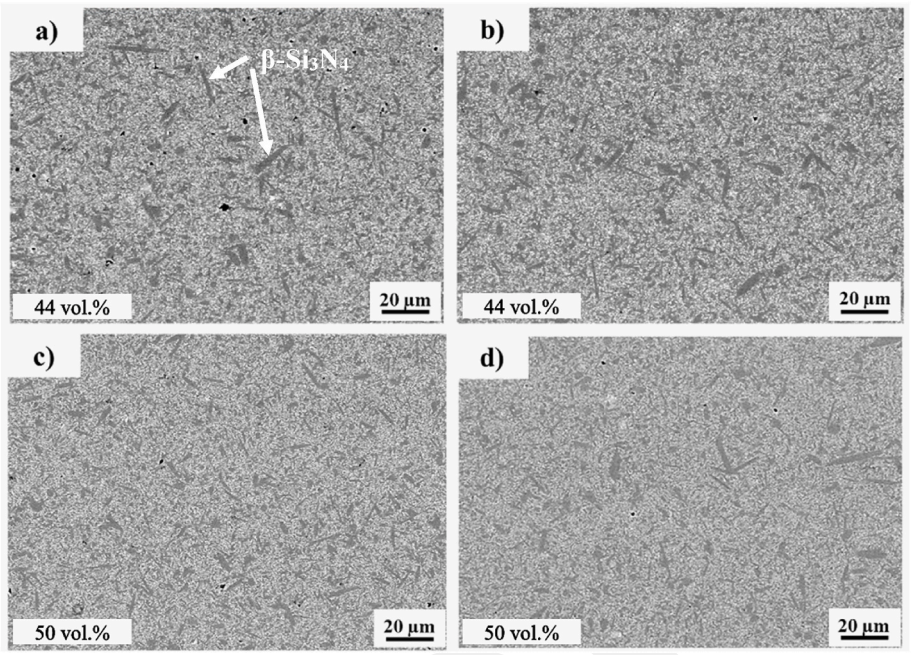


**Fig. 9.** BSE-SEM images of sintered samples at differant solid loading (a, c) after DCC, (b, d) after DCC + CIP.

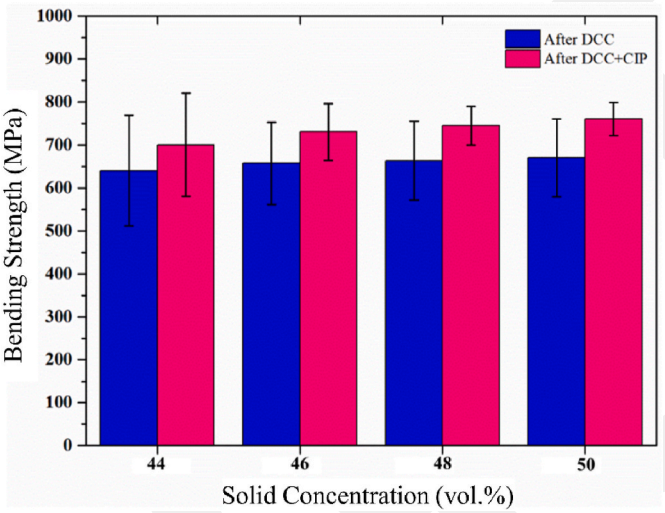


**Fig. 10.** The effect of CIP and solid concentrations on the bending strength of sintered $Si_3N_4$ specimens.

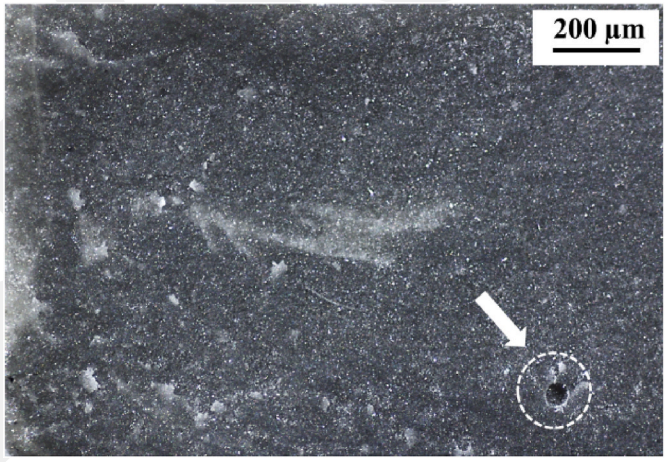


**Fig. 11.** Defects in the form of circular pores in the sintered specimen at 50 vol. % solid content (circled).

used and the densities were over 98.5% for suspensions 46 vol.%. The highest density of 99.2% was achieved when 50 vol.% suspension was used. The DCC + CIP samples are all sintered to over 99% relative density. The lowest density was 99.3% with 44 vol.% suspension while the highest was 99.7% for the sample with 50 vol.% solid loading. Although applying 200 MPa CIP reduced the density differences between different particle volume loading samples, it did not completely eliminated the differences. Densification behaviours at different particle volume loadings of DCC and DCC + CIP samples clearly support the green microstructure observations (Fig. 6).

### 3.3. Phase composition and microstructure of sintered bodies

The XRD patterns of green and sintered $Si_3N_4$ specimens produced by using the suspension with 50 vol.% solids concentration is shown in Fig. 8. It was observed that α-$Si_3N_4$ was completely transformed into β-$Si_3N_4$ phase after sintering at 1950 °C, which was expected at this high sintering temperature. The unmarked peaks in Fig. 8b are probably due to the crystalline phases forming in the microstructure due to sintering additives.

The SEM images of the polished surfaces of $Si_3N_4$ sintered samples produced at 44 and 50 vol.% solid loading are given in Fig. 9. It was observed that β-$Si_3N_4$ elongated grains with high length to diameter ratio were formed in all specimens without any noticeable differences between the different volume loadings. Higher porosity is evident from sample with 44 vol.% solid loading (Fig. 9a) and should result from the larger pores between the aggregates shown in Fig. 6a due to the formation of larger flocs during the coagulation process. CIP helps to reduce the size and amount of the porosity, also after sintering (Fig. 9b). On the contrary, comparison of Fig. 9c and d indicates that the difference in the amount of porosity between DCC and DCC + CIP samples after sintering was lower at 50 vol.% suspension due to the lower inter-aggregate porosity of the green bodies at this concentration.

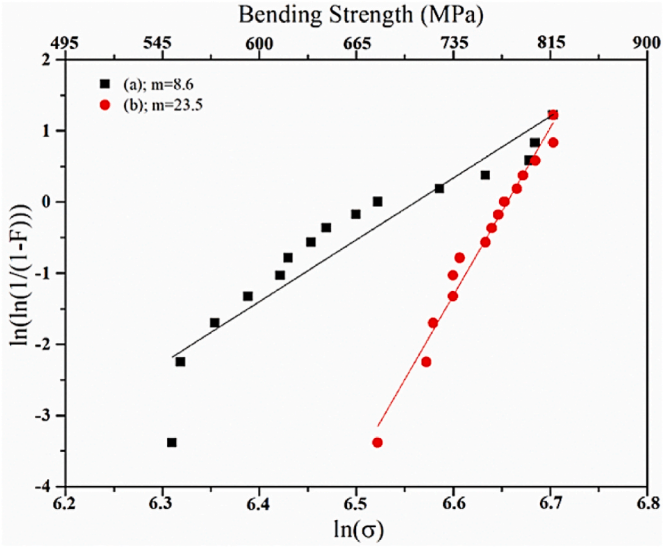


**Fig. 12.** Weibull distributions of bending strength of sintered samples with 50 vol.% solid loading (a) after DCC; (b) after DCC + CIP.

### 3.4. Mechanical properties of $Si_3N_4$ sintered bodies

With the increase of the solid volume loading from 44 vol.% to 50 vol.%, Vickers hardness and fracture toughness values of the DCC samples increased from 13.7 to 14.2 GPa and from 6.75 to 7.00 MPa•$m^{1/2}$, respectively, and those of the DCC + CIP samples increased from 14.1 to 14.4 GPa and from 6.81 to 7.10 MPa•$m^{1/2}$. This increase may be attributed to the increase in sintered density.

Bending strengths of $Si_3N_4$ ceramic parts produced by DCC and DCC + CIP by using different particle volume loading suspensions are given in Fig. 10. The average strength values of DCC samples change between 640 ± 129 MPa to 670 ± 90 MPa as the particle volume loading of suspensions increased from 44 vol.% to 50 vol.%. Neither the strength nor the scatter in the strength values changed significantly for DCC samples. This indicates that particle volume loading of the suspension does not change the size and the distribution of defects significantly. Considering that toughness of the $Si_3N_4$ material is 7 MPa•$m^{1/2}$ and that pores are circular, the critical pore size of about 75 μm can be calculated from Griffith equation [35] at 650 MPa strength. Fig. 11 shows such a circular pore on the fracture surface of bending sample. These pores clearly result form trapped air bubbles during suspension preparation and/or casting and it appears that the vacuum treatment is not enough to remove them completely.

Application of CIP on DCC samples not only improves the strength but also reduces the scattering in the strength values and this scatter is the lowest when 50 vol.% particle loading suspension is used. The average strength values of DCC + CIP samples change between 700 ± 120 MPa to 760 ± 39 MPa as the particle volume loading of suspensions increased from 44 vol.% to 50 vol.%. Fig. 12 shows the Weibull graph of DCC and DCC + CIP samples prepared from 50 vol.% particle loading suspension. The average strength value and Weibull modulus ($m$) of DCC samples were 670 MPa and 8.6, respectively and those of DCC + CIP samples were 760 MPa and 23.5. Improvement in reliability with the application of CIP is evident. There has been no report on $m$ values of $Si_3N_4$ ceramics produced by the DCC method. However, Zhou et al. [24] reported a little higher $m$ value (12.4) of a $Si_3N_4$ produced by gel casting and also found that CIP somewhat improves the $m$ value over 15. It is to be noted that the most common Weibull modulus values for technical ceramics lie between 5 and 22 depending on the production methods and processing conditions [36]. With this respect, while DCC itself may be prone to processing defects like air bubbles, it can be a good method to obtain reliable and complex shape $Si_3N_4$ ceramics when combined with CIP.

## 4. Conclusions

In this study, direct coagulation casting of silicon nitride suspensions at different particle volume loading was reported. Green densities close to the suspension particle volume loading were obtained. It was observed that suspension particle loading affects the hierarchy of the particles in the green body. Sintering to near full density was achieved, particularly when a suspension with high particle volume loading was used. However, the sintered parts at 50 vol.% solid content have relatively low average bending strength (670 ± 90 MPa) with a rather large scatter in strength values and corresponding lower Weibull modulus ($m$= 8.6). The reason for the lower mechanical properties is attributed to larger circular pores which are due to trapped air bubbles in the suspension. However, cold isostatic pressing of the DCC shaped parts reduced the size and amount of pores and gave rise to the increased relative density above 99.5%, average bending strength (760 ± 39 MPa) and Weibull modulus ($m$= 23.5). Therefore, direct coagulation casting combined with cold isostatic pressing could be a viable route to produce complex shaped $Si_3N_4$ ceramics.

## CRediT authorship contribution statement

**Hande Marulcuoglu:** Conceptualization, Investigation, Methodology, Validation, Visualization, Writing – original draft. **Ferhat Kara:** Supervision, Writing – review & editing, Funding acquisition, Project administration.

## Declaration of competing interest

The authors declare that they have no known competing financial interests or personal relationships that could have appeared to influence the work reported in this paper.

## Data availability

The raw/processed data required to reproduce these findings cannot be shared at this time due to technical or time limitations.

## Acknowledgements

This study was supported by the Eskisehir Technical University Scientific Research Projects under the project number of 1610F666. Authors are grateful for the MDA Advanced Ceramics Ltd. for supplying all the raw materials for the fabrication of $Si_3N_4$ ceramic materials.

## References

[1] H.M. Bernal, B. Matovic, Mechanical properties of silicon nitride-based ceramics and its use in structural applications at high temperatures, Mater. Sci. Eng., A 527 (2010) 1314–1338, https://doi.org/10.1016/j.msea.2009.09.064.
[2] M.J. Hoffmann, G. Petzow, Tailored microstructures of silicon nitride ceramics, Pure Appl. Chem. 66 (9) (1994) 1807–1814, https://doi.org/10.1351/pac199466091807.
[3] G. Ziegler, J. Heinrich, G. Wötting, Review relationships between processing, microstructure and properties of dense and reaction-bonded silicon nitride, J. Mater. Sci. 22 (1987) 3041–3086, https://doi.org/10.1007/BF01161167.
[4] X. Quin, S. Li, L. Zhao, L. Sheng, Z. Xie, Silicon nitride ceramics consolidated by oscillatory pressure sintering, Ceram. Int. 46 (2020) 14235–14240, https://doi.org/10.1016/j.ceramint.2020.02.021.
[5] X. Zhu, Y. Sakka, Textured silicon nitride: processing and anisotropic properties, Sci. Technol. Adv. Mater. 9 (2008) 1–47, https://doi.org/10.1088/1468-6996/9/3/033001.
[6] G. He, A.D. Hirschfeld, J. Cesarano III, J.N. Stuecker, Processing of Silicon Nitride Ceramics from Concentrated Aqueous Suspensions by Robocasting, 2000. SANO2000-2055J.
[7] W. Li, H. Zhang, Y. Jin, M. Gu, Rapid coagulation of silicon carbide slurry via direct coagulation casting, Ceram. Int. 30 (2004) 411–416, https://doi.org/10.1016/S0272-8842(03)00125-1.

[8] J. Yang, J. Yu, Y. Huang, Recent developments in gelcasting of ceramics, J. Eur. Ceram. Soc. 31 (2011) 2569–2591, https://doi.org/10.1016/j.jeurceramsoc.2010.12.035.
[9] L. Montanaro, B. Coppola, P. Palmero, J.M. Tulliani, A review on aqueous gelcasting: a versatile and low-toxic technique to shape ceramics, Ceram. Int. 45 (2019) 9653–9673, https://doi.org/10.1016/j.ceramint.2018.12.079.
[10] A.N. Chen, J.M. Wu, L.X. Han, L.J. Cheng, R.Z. Liu, X.Y. Zhang, Y.S. Shi, C.H. Li, Preparation of $Si_3N_4$ foams by DCC method via dispersant reaction combined with protein-gelling, J. Alloys Compd. 745 (2018) 262–270, https://doi.org/10.1016/j.jallcom.2018.02.238.
[11] J.M. Wu, W.Z. Lu, X.H. Wang, P. Fu, M. Ni, J.L. Yang, C. Wang, Q.C. Zeng, $Ba_{0.6}Sr_{0.4}TiO_3$-MgO ceramics from ceramic powders prepared by improved aqueous gelcasting-assisted solid-state method, J. Eur. Ceram. Soc. 33 (2013) 2519–2527, https://doi.org/10.1016/j.jeurceramsoc.2013.04.015.
[12] J.A. Lewis, Colloidal processing of ceramics, J. Am. Ceram. Soc. 83 (10) (2000) 2341–2359, https://doi.org/10.1111/j.1151-2916.2000.tb01560.x.
[13] T.J. Graule, F.H. Baader, L.J. Gauckler, Casting uniform ceramics with direct coagulation, Chemtech 25 (6) (1995) 31–37.
[14] M.W. Sigmund, S.N. Bell, S.N. Bergström, Novel Powder-processing methods for advanced ceramics, J. Am. Ceram. Soc. 83 (7) (2000) 1557–1574, https://doi.org/10.1111/j.1151-2916.2000.tb01432.x.
[15] K. Gan, J. Xu, X. Zhang, W. Huo, M. Yang, Y. Qu, J. Yang, Direct coagulation casting of silicon nitride suspension via a dispersant reaction method, Ceram. Int. 42 (2016) 4347–4353, https://doi.org/10.1016/j.ceramint.2015.11.113.
[16] W. Si, T.J. Graule, F.H. Baader, L.J. Gauckler, Direct coagulation casting of silicon carbide components, J. Am. Ceram. Soc. 82 (5) (1999) 1129–1136, https://doi.org/10.1111/j.1151-2916.1999.tb01886.x.
[17] K. Gan, J. Xu, Y. Lu, X. Zhang, W. Huo, J. Yang, Preparation of silicon carbide ceramics using chemical treated powder by DCC via dispersant reaction and liquid phase sintering, J. Eur. Ceram. Soc. 37 (2017) 891–897, https://doi.org/10.1016/j.jeurceramsoc.2016.10.009.
[18] M.J. Wu, X.Y. Ma, J.L. Cheng, N.A. Chen, S. Chen, W. Wang, Z.R. Liu, S.Y. Shi, H. C. Li, Isotropic $Si_3N_4$ ceramics fabricated by low-pressure spark plasma sintering in combination with direct coagulation casting, Ceram. Int. 45 (2019) 8454–8459, https://doi.org/10.1016/j.ceramint.2019.01.155.
[19] X.J. Liu, L.P. Huang, H.C. Gu, X. Xu, X.R. Fu, Direct coagulation casting of silicon nitride ceramics, J. Inorg. Mater. 16 (2001) 877–882, https://doi.org/10.3321/j.issn:1000-324X.2001.05.016.
[20] J. Zhang, D. Jiang, Q. Lin, Z. Chen, Z. Huang, Properties of silicon carbide ceramics from gelcasting and pressureless sintering, Mater. Des. 65 (2015) 12–16, https://doi.org/10.1016/j.matdes.2014.08.034.
[21] T. Zhang, Z. Zhang, J. Zhang, D. Jiang, Q. Lin, Preparation of SiC ceramics by aqueous gelcasting and pressureless sintering, Mater. Sci. Eng., A 443 (2007) 257–261, https://doi.org/10.1016/j.msea.2006.08.047.
[22] Y. Huang, L.G. Ma, Q. Tang, J.L. Yong, Z.P. Xie, X.L. Xu, Surface oxidation to improve water-based gelcasting of silicon nitride, J. Mater. Sci. 35 (2000) 3519–3524, https://doi.org/10.1023/A:1004897026241.
[23] Y. Huang, L.J. Zhou, Q. Tang, Z.P. Xie, J.L. Yang, Water-based gelcasting of surface coated silicon nitride powder, J. Am. Ceram. Soc. 83 (4) (2001) 701–707, https://doi.org/10.1111/j.1151-2916.2001.tb00729.x.
[24] L. Zhou, Y. Huang, Z. Xie, A. Zimmermann, F. Aldinger, Preparation of $Si_3N_4$ ceramics with high strength and high reliability via a processing strategy, J. Eur. Ceram. Soc. 22 (2002) 1347–1355, https://doi.org/10.1016/S0955-2219(01)00438-1.
[25] H. Marulcuoglu, Shaping of $Si_3N_4$ Ceramics with Wet Methods, PhD Thesis, Eskisehir Technical University, Institute of Graduate Programs, 2019.
[26] E. Rocha-Rangel, Fracture toughness determinations by means of ındentation fracture, in: J. Cuppoletti (Ed.), Nanocomposites with Unique Properties and Applications in Medicine and Industry, vols. 21–38, Intech, 2011, ISBN 978-953-307-351-4.
[27] J. Zhang, F. Ye, D. Jiang, M. Iwasa, Dispersion of $Si_3N_4$ powders in aqueous media, Colloids Surf. A Physicochem. Eng. Asp. 259 (2005) 117–123, https://doi.org/10.1016/j.colsurfa.2005.02.006.
[28] R.R. Rao, H.N. Roopa, T.S. Kannan, pH controlled dispersion and slip casting of $Si_3N_4$ in aqueous media, Bull. Mater. Sci. 24 (1) (2001) 57–61, https://doi.org/10.1007/BF02704841.
[29] W. Li, P. Chen, M. Gu, Y. Jin, Effect of TMAH on rheological behavior of SiC aqueous suspension, J. Eur. Ceram. Soc. 24 (2004) 3679–3684, https://doi.org/10.1016/j.jeurceramsoc.2003.12.023.
[30] A.J. Millan, M.I. Nieto, R. Moreno, Aqueous injection moulding of silicon nitride, J. Eur. Ceram. Soc. 20 (2000) 2661–2666, https://doi.org/10.1016/S0955-2219(00)00118-7.
[31] R. Moreno, A. Salomoni, S.M. Castanho, Colloidal filtration of silicon nitride aqueous slips. Part I: optimization of the slip parameters, J. Eur. Ceram. Soc. 18 (1998) 405–416, https://doi.org/10.1016/S0955-2219(97)00133-7.
[32] M.P. Albano, L.B. Garrido, Concentrated aqueous $Si_3N_4$ –$Y_2O_3$ –$Al_2O_3$ slips stabalized with tetramethylammonium hydroxide, Cerâmica 45 (295) (1999), https://doi.org/10.1590/S0366 69131999000500002.
[33] S. Yin, S. Jiang, L. Pan, L. Guo, Z. Zhang, J. Zhang, X. Li, T. Qui, J. Yang, Effects of solid loading and calcination temperature on microstructure and properties of porous $Si_3N_4$ ceramics by aqueous gelcasting using DMAA system, Ceram. Int. 45 (2019) 19925–19933, https://doi.org/10.1016/j.ceramint.2019.06.250.
[34] P.J. Flory, Principles of Polymer Chemistry, Cornell University Press, London, 1953.
[35] C. Kawaı, Effect of grain size distribution on the strength of porous $Si_3N_4$ ceramics composed of elongated β-$Si_3N_4$ grains, J. Mater. Sci. 36 (2001) 5713–5717, https://doi.org/10.1023/A:1012542421983.
[36] S. Bueno, C. Baudin, Mechanical behaviour of structural ceramics, Bol. Soc. Esp. Ceram. V. 46 (3) (2007) 103–118.